nature climate change

SUPPLEMENTARY INFORMATION

DOI: 10.1038/NCLIMATE1456

Evaluation of climate models using palaeoclimatic data

Pascale Braconnot[1], Sandy P. Harrison[2], Masa Kageyama[1], Patrick J. Bartlein[3], Valerie Masson-Delmotte[1], Ayako Abe-Ouchi[4], Bette Otto-Bliesner[5], Yan Zhao[2]

1. IPSL/ Laboratoire des Sciences du Climat et de l'Environnement, unité mixte de recherches CEA-CNRS-UVSQ, Orme des Merisier, bât 712, 91191 Gif sur Yvette Cedex, France.
2. School of Biological Sciences, Macquarie University, North Ryde, NSW 2109, Australia.
3. Department of Geography, University of Oregon, Eugene, Oregon, USA
4. Center for Climate System Research, University of Tokyo, Japan
5. Climate and Global Dynamics Division, National Center for Atmospheric Research, Boulder, USA

The SI contains (a) a summary of the boundary conditions for the Mid-Holocene (MH, ca 6 ka) and Last Glacial Maximum (LGM, ca 21 ka) experiments, (b) descriptions about the data sets available for the Mid-Holocene (MH, ca 6 ka) and Last Glacial Maximum (LGM, ca 21 ka) for model evaluation and benchmarking in CMIP5, and (c) estimates of shortwave forcing and feedbacks at the Last Glacial Maximum (LGM, ca 21 ka).

Boundary conditions for the MH and LGM experiments in PMIP1, PMIP2 and PMIP3

Mid-Holocene (MH) and Last Glacial Maximum (LGM) simulations are equilibrium experiments, presenting a "snapshot" of climate at a specific time. The table S1 shows the boundary conditions used for MH and LGM experiments during the various phases of the Palaeoclimate Modelling Intercomparison Project (PMIP). The ultimate external forcing (or driver) of climate is change in incoming solar radiation (insolation) as determined by changes in the Earth's orbit. These changes can be specified precisely [1]. Due to the slow variations of Earth's orbital parameters, the seasonal and latitudinal distribution of MH insolation was different from present (1950 C.E), enhancing the magnitude of the seasonal contrast in the Northern Hemisphere by about 60Wm^{-2}. Insolation forcing at the LGM was very similar to present. When models do not explicitly simulate slow processes such as the build up of ice sheets, concomitant changes in land-sea distribution, or the evolution of atmospheric

composition, all of which lead to changes that have to be considered as climate forcings on shorter timescales, then these boundary conditions (hereafter forcings) have to be prescribed in the MH and LGM experiments. As models have evolved in complexity, so the set of forcings that has to be prescribed has also evolved. In the first phase of the Palaeoclimate Modelling Intercomparison Project (PMIP1), the experiments were performed with atmospheric general circulation models and the state of the ocean was prescribed as a forcing. In the second phase of PMIP (PMIP2), some models incorporated vegetation dynamics but vegetation cover and albedo still had to be specified for the coupled ocean-atmosphere general circulation models (OAGCMs). Some processes, such as those associated with the terrestrial and marine carbon cycle, have been ignored in the earlier PMIP experiments, but will be included as interactive components of some of the models used in PMIP3. In all experiments the atmospheric composition is prescribed using results from ice-cores [2,3,4,5].

Table S1: Evolution of the boundary conditions prescribed in the different phase of the PMIP project. Boundary conditions that remain the same between different sets of simulations are highlighted in yellow; blue highlighting shows boundary conditions that are not included in a given set of experiments. More details of the protocols to be used in PMIP3 can be found on the PMIP3 web site (see http://pmip3.lsce.ipsl.fr/), which also provides links to the webpages detailing the protocols used in PMIP1 and PMIP2. Note that in the MH experiment the CO2 concentration is the pre-industrial one. CO2ctrl refers to the CO2 concentration of the control simulation.

	PMIP1	PMIP2	PMIP3
Mid Holocene (6000 years BP)* *In this experiment ice-sheet, coastline, solar constant and aerosols are prescribed as in the PI simulation.			
Insolation	**eccentricity** = 0.018682 **obliquity** = 24.105° **perihelion-180°** = 0.87°	**eccentricity** = 0.018682 **obliquity** = 24.105° **perihelion-180°** = 0.87°	**eccentricity** = 0.018682 **obliquity** = 24.105° **perihelion-180°** = 0.87°
Trace gases	**CO_2** = 280 ppm Or 280/345* CO_2ctrl **CH_4** = 650 ppb **N_2O** = 270 ppb **CFC** = 0 **O_3** = not considered	**CO_2** = 280 ppm **CH_4** = 650 ppb **N_2O** = 270 ppb **CFC** = 0 **O_3** = not considered	**CO_2** = 280 ppm **CH_4** = 650 ppb **N_2O** = 270 ppb **CFC** = 0 **O_3** = same as in CMIP5 PI
Vegetation and land surface	Prescribed to be the same as modern vegetation	Either prescribed to be the same as modern vegetation or computed using a dynamical vegetation module	Computed using a dynamical vegetation module, or prescribed as in PI, with phenology computed for models with active carbon cycle or prescribed from data
Carbon cycle	Not considered	Not considered	Interactive, with atmospheric concentration prescribed and ocean and land carbon fluxes diagnosed as recommended in CMIP5
Last Glacial Maximum (21000 years BP) * * In this experiment solar constant and aerosols are prescribed as in the PI simulations.			
Insolation	**eccentricity** = 0.018994 **obliquity** = 22.949° **perihelion-180°** = 114.42°	**eccentricity** = 0.018994 **obliquity** = 22.949° **perihelion-180°** = 114.42°	**eccentricity** = 0.018994 **obliquity** = 22.949° **perihelion-180°** = 114.42°
Trace gases	**CO_2** = 200 ppm or (200/280) * CO_2ctrl **CH_4** = 350 ppb **N2O** = 190 ppb **CFC** =0 **O_3** = same as in PI	**CO_2** = 185 ppm **CH_4** = 350 ppb **N_2O** = 200 ppb **CFC** =0 **O_3** = same as in PI	**CO_2** = 185 ppm **CH_4** = 350 ppb **N_2O** = 200 ppb **CFC** =0 **O_3** = same as in PI
Ocean	SST prescribed from CLIMAP (1981) Or SST computed using a slab ocean model	3D Ocean model and sea-ice	3D ocean model and sea-ice
Ice sheet	Peltier et al (1994) [6]	Peltier et al (2004) [7]	Blended ice sheet
Land-sea mask	- 105 m sea level	Prescribed following Peltier (2004) [7] land-sea mask -120 m	Prescribed from the blended ice-sheet land-sea mask. Sea-level change consistent with the change in land-sea mask.
Freshwater		Excess LGM freshwater added to the ocean in 3 different regions	Excess LGM freshwater added to the ocean
Ice sheet ice streams	Not considered	Not considered	Not considered
River runoff	Not considered	As in CTRL or river pathway modified	As in PI or river pathway modifier according to PMIP protocol
Mean ocean salinity	Not considered	Not considered	+1 PSU everywhere
Carbon cycle	Not considered	Not considered	Interactive, with atmospheric concentration prescribed and ocean and land carbon fluxes diagnosed as recommended in CMIP5 For PCMIP: fully interactive with atmospheric concentration computed by the model

Data syntheses for the mid-Holocene and the Last Glacial maximum

The focus of PMIP (and other palaeoclimatic modelling efforts) on the MH and LGM has motivated both regional and global syntheses of palaeoenvironmental and palaeoclimatic data, and the development of benchmark data sets. Here we illustrate the global subset of these data sets.

The Global Lake Status Data Base

The Global Lake Status Data Base (GLSDB) [8] was the product of an international effort to compile the geomorphic and biostratigraphic data for changes in lake status (a measure of relative changes in lake level, water depth or lake volume through time), in order to document changes in regional water balance during the last 30,000 years. The change in lake status provides a qualitative estimate of the change in water balance (precipitation minus evaporation, P-E) over the lake and its catchment [9] and can be compared to simulated P-E [10]. The MH lake status map shows large-scale increases in P-E compared to present in regions affected by the northern hemisphere monsoons [8] (Figure S1a). Smaller-scale regional patterns, such as the drier condition around the Baltic Sea, have also been interpreted as reflecting changes in regional water balance consequent on changes in atmospheric circulation patterns [11]. The LGM lake status map shows conditions drier than present almost everywhere (Figure S1b), except in those regions such as western North America and the circum-Mediterranean which were subject to increased precipitation in consequence of the southward displacement of the westerlies by the Laurentide ice sheet [8].

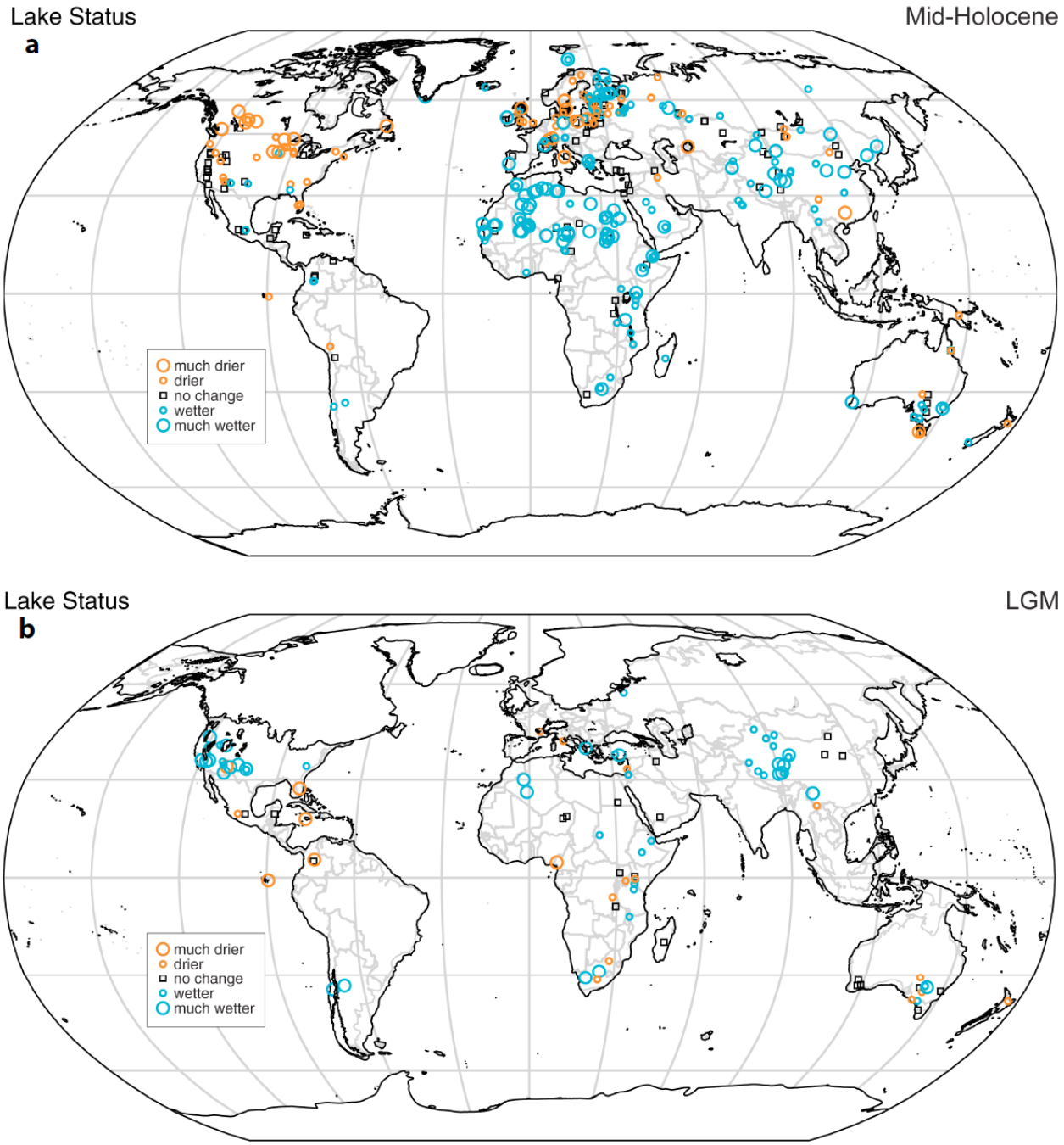

Figure S1: Differences in lake status between (a) the mid-Holocene and (b) the LGM, and the present-day lake status of an individual lake. For mapping purposes, the relative lake status through time is classified into three categories (high, intermediate, low – which includes intervals when the lake was dry), which following Street-Perrott and Harrison [12] represents a roughly equal proportion of the history of an individual lake. The map uses a Robinson projection centred on 0°, 0°; the grid lines are every 30°.

The BIOME 6000 project.

The BIOME 6000 project is a long-standing initiative of the International Geosphere-Biosphere Programme (IGBP)[13] to map past vegetation patterns based on fossil-pollen and plant-macrofossil samples. The taxa represented in each pollen or macrofossil assemblage are assigned to plant functional types (PFTs) on the basis of current information about the life form, phenology and physiology of the constituent species; major vegetation types (biomes) are defined in terms of the presence/absence of PFTs; scores of the affinity of each pollen or macrofossil assemblage to each biome are calculated based on these two classifications and the sample is then assigned to the biome with which it has the greatest affinity [14]. This method has been applied to construct regional biome maps [15,16,17,18,19]. During the MH, woody vegetation expanded into areas now occupied by deserts in response to the orbitally-induced expansion of the northern hemisphere monsoons; northward expansion of forests in eastern Canada and Eurasia reflects high latitude warming (Figure S2). At the LGM, forests disappeared over much of Eurasia as a consequence of colder condition (Figure S2). The BIOME 6000 maps provide targets for evaluation of coupled models that include vegetation dynamics [20], but they can also be compared to the output of vegetation models driven by output from coupled climate models [21 22].

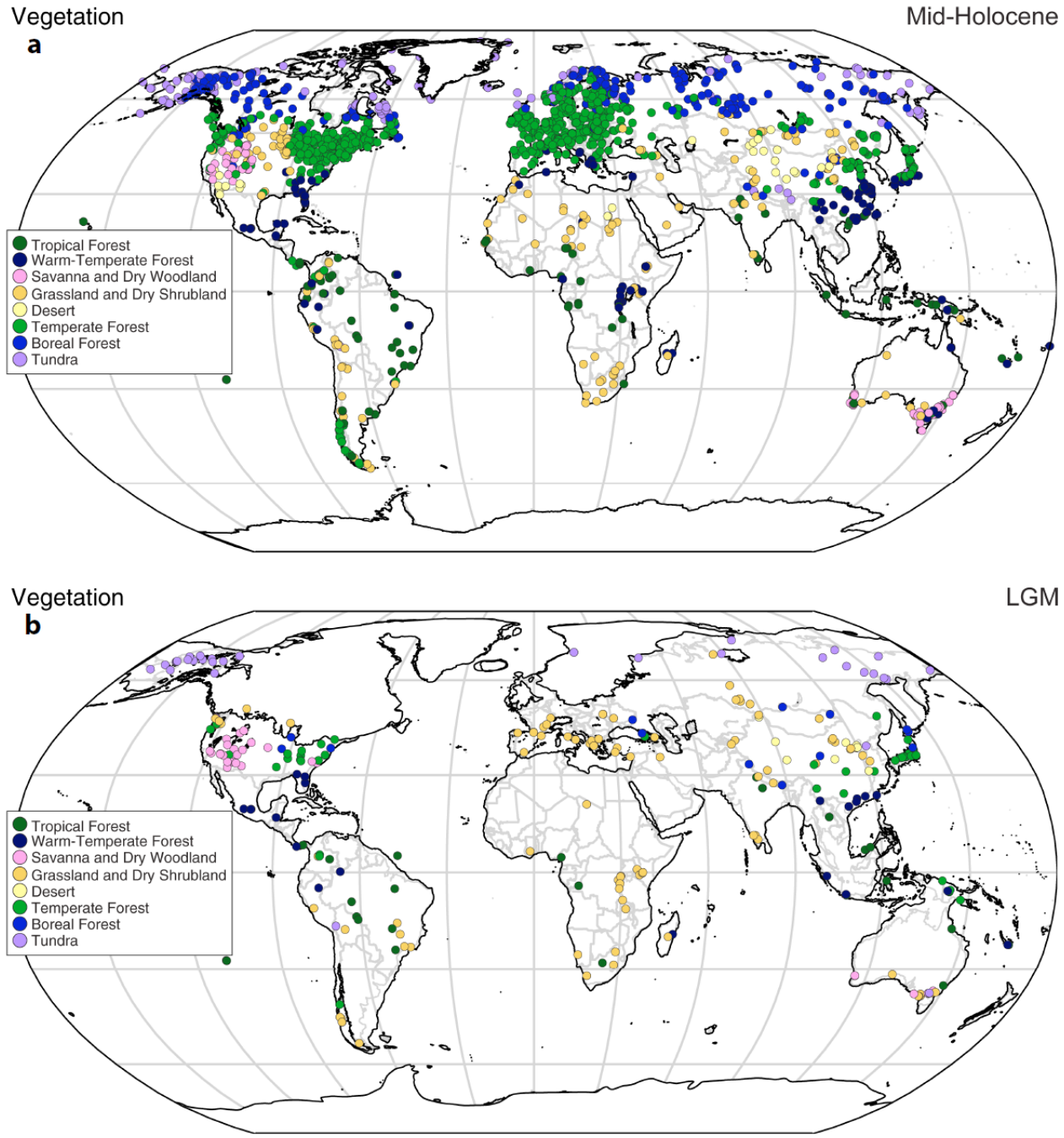

Figure S2: The latest update of the BIOME 6000 data set, showing vegetation reconstructions for (a) MH (Harrison and Prentice, unpublished data) and (b) LGM [23]. In order to construct global maps, the PFT and biome terminology used in each region has been standardised.

Sedimentary charcoal records

Sedimentary charcoal records from e.g. lakes, bogs, and marine cores provide a record of biomass burning, which approximates the amount of biomass lost in wildfires [24]. The IGBP-sponsored Global Palaeofire Working Group (GPWG) has assembled charcoal records from nearly 800 sites globally. Charcoal is obtained from a wide range of depositional environments, at varying temporal resolution or sampling intervals, and is quantified using a variety of different metrics. For comparison between sites, the data are therefore standardized using a standard procedure which involves (1) transforming non-influx data (e.g. concentration expressed as particles/cm^3) to influx values (i.e. particles/cm^2/yr) or quantities proportional to influx, by dividing the charcoal values by sample deposition times, (2) homogenising the variance using the Box-Cox transformation, (3) rescaling the values using a minimax transformation to allow comparisons among sites, and (4) rescaling values once more to z-scores using a base period of 21 to 0.2 ka [25]. Analyses of the impacts of each of these procedures on the records have shown that the relationship between the original and standardized record from a site is linear or monotonic [25,26]. Figure S3b shows that at the LGM, biomass burning was generally reduced compared to present; the Holocene (Figure S3a) was characterised by increased fire activity, although at sub-continental scales these patterns are complicated by regional climate controls (see Power et al. [24], for further discussion of these patterns). As with the vegetation data (Figure S2), the biomass-burning reconstructions provide targets for coupled models that include fire disturbance impacts on dynamic vegetation [27] but they can also be compared to the output of fire-enabled vegetation models [28] driven by output from coupled climate models.

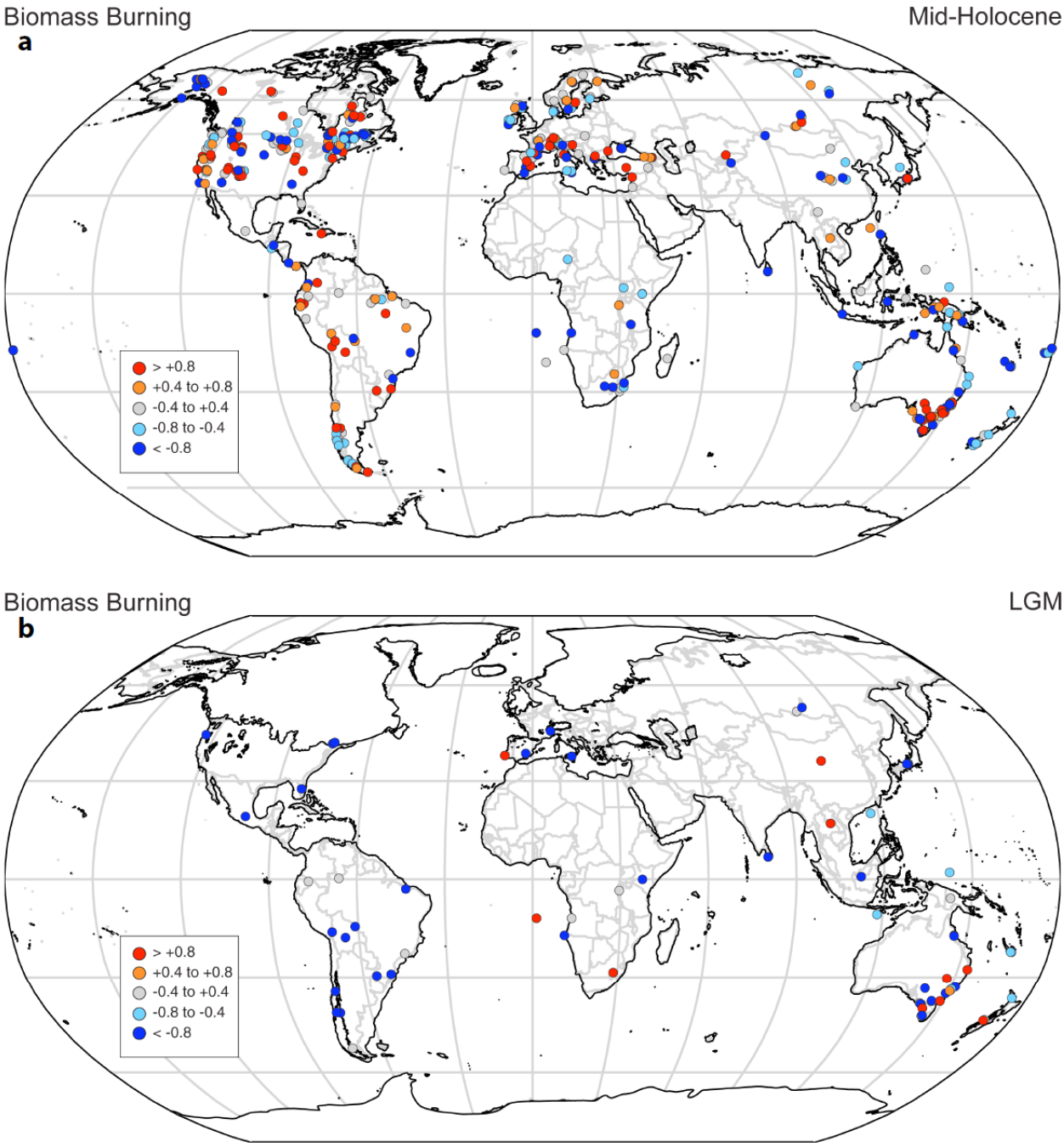

Figure S3: Changes in biomass burning at (a) the MH and (b) the LGM, expressed as z-scores of transformed charcoal influx (see text for details), from the Global Palaeofire Working Group Database (Version 2, unpublished data).

The DIRTMAP database

Changes in dust affect the radiation budget, and account for about -1Wm^{-2} in the radiative perturbation of the LGM [29,30]. This forcing is not currently included in the PMIP3 simulations, but sensitivity experiments will be run by a subset of PMIP modelling groups. The DIRTMAP (Dust Indicators and Records from Terrestrial and MArine Palaeoenvironments) database contains records of dust accumulation rates ($g/m^2/yr$) from ice and marine cores, and terrestrial deposits. Dust deposition, and hence atmospheric dust loading, was between 2-5 greater at the LGM than today with largest increases associated with the expansion of arid lands in Africa and Asia (Figure S4). This map serves as a target for coupled models that explicitly simulate dust transport and deposition, but can also be compared to the output of offline dust models [31] driven by output from coupled climate models to test if the changes in the atmospheric circulation produced for the LGM is compatible with observed changes in dust accumulation.

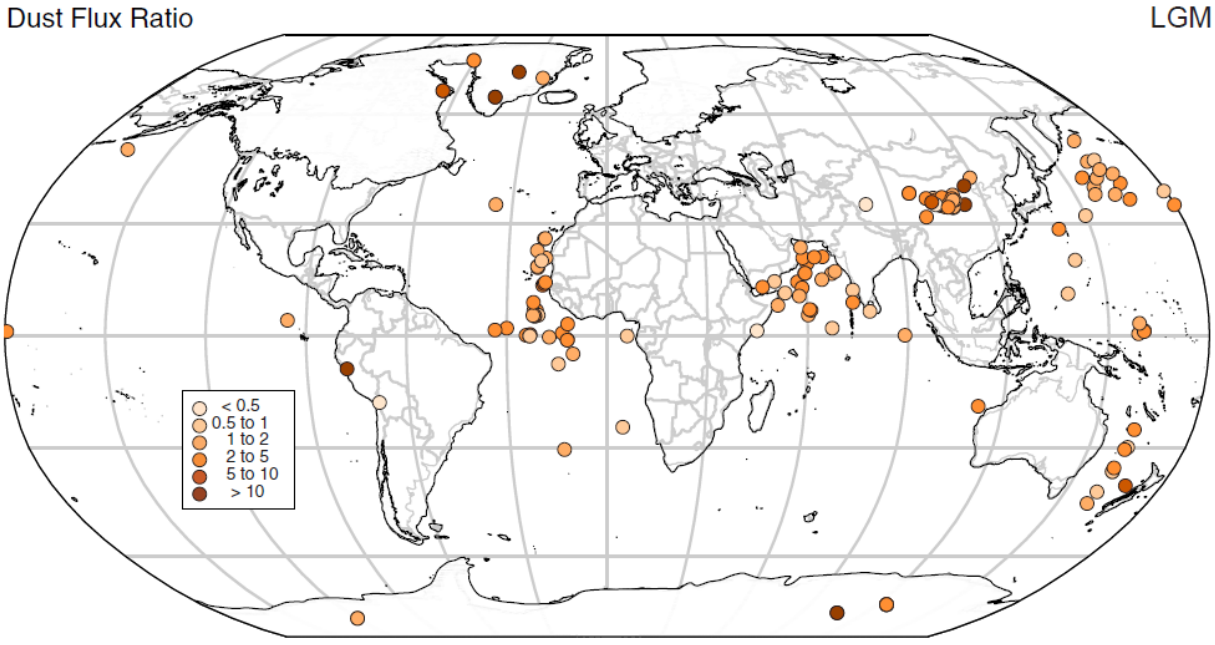

Figure S4: Changes in dust deposition at the LGM, expressed as the ratio compared to present deposition, from version 2 of the DIRTMAP dataset [32,33].

Reconstruction of bioclimatic variables over land

Pollen and plant macrofossil data are an important resource from which climatic (e.g. mean annual temperature) or bioclimatic (e.g. the accumulated temperature during the growing season) variables can be estimated using different statistical and inverse-modelling methods. A global synthesis of various regional data sets for the MH and LGM has been assembled by a PMIP working group (Bartlein et al [34]) and provides reconstructions of six variables: mean temperature of the warmest month (MTWA), the accumulated temperature sum during the growing season (growing degree days above a baseline temperature for the growth of woody plants of 5°C**:** GDD5), mean temperature of the coldest month (MTCO), mean annual temperature (MAT), mean annual precipitation (MAP) and the ratio of equilibrium to potential evapotranspiration (α) for each period. This dataset also include uncertainties arising from data resolution and sampling, age scale uncertainties, analytical uncertainties and calibration model uncertainty. To facilitate comparison with climate-model outputs, the variables are presented as gridded anomalies on a regular latitude/longitude grid of 2° by 2° (comparable to the typical grid size of the PMIP models). The grid-cell value of the anomaly was obtained by simple averaging and that for the uncertainty as a pooled estimate of the standard error. Analyses of these data have shown that methodological uncertainties have little impact on the reconstructions: the reconstructed climate variables show large, spatially coherent patterns that are consistent with plausible responses to known climate forcing. Figure S5 shows MAT anomalies for the MH and LGM, as an example of this data set,.

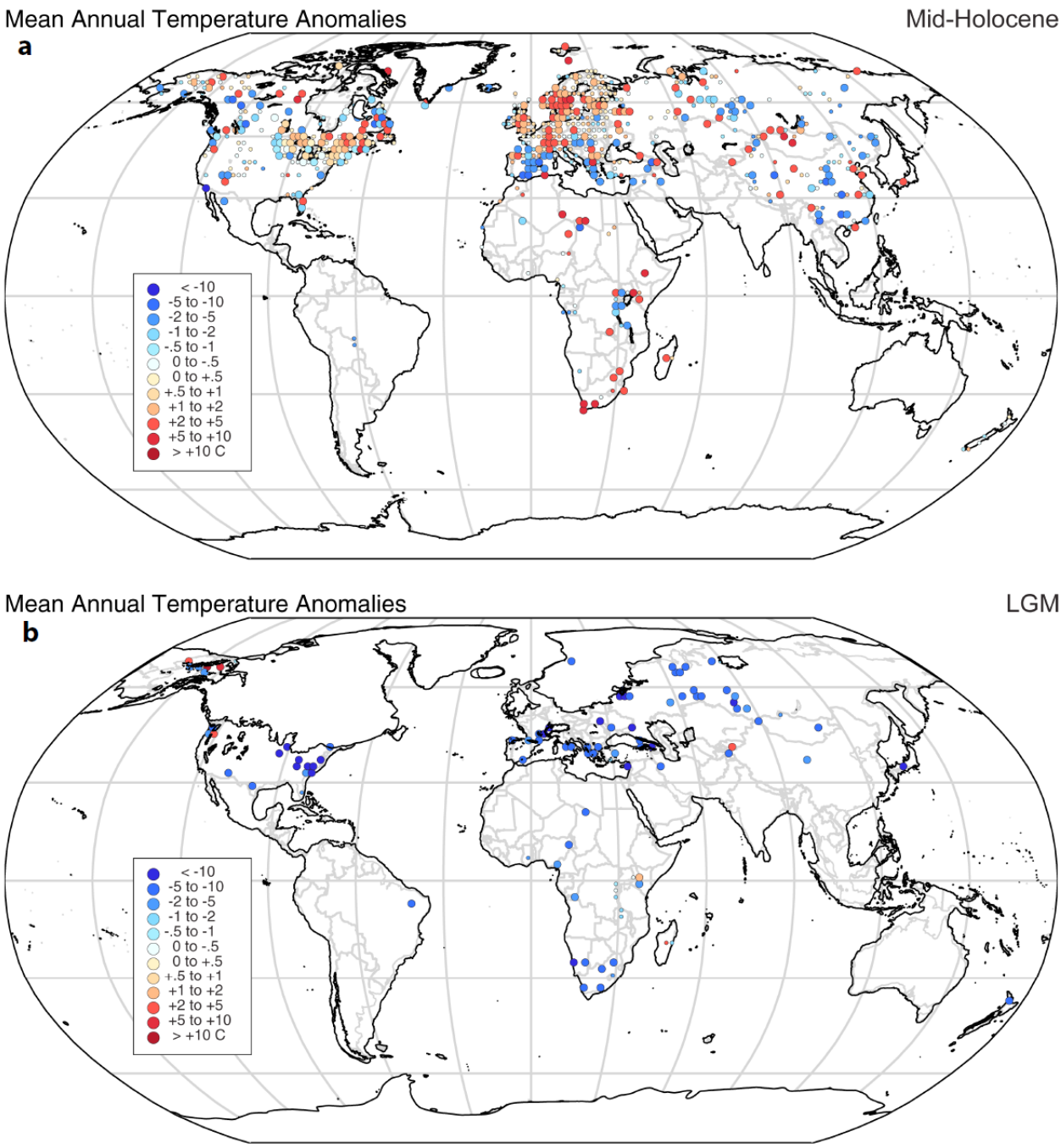

Figure S5: Changes in mean annual temperature (°C) for (a) the MH and (b) the LGM, compared to present, from pollen and plant macrofossil data[34]. The size of the circles shows the statistical confidence attached to the individual grid-cell reconstructions, with small circles showing that the cell values are not individually statistically significant. The spatial coherence of the patterns shown, however, makes it clear that standard measures of significance are too conservative.

Temperature reconstruction over the ocean

Reconstructions of seasonal sea-surface temperatures (SST) and seasonal sea-ice cover have been developed by the paleoceanographic community using biological and geochemical evidence from deep-sea sediments. The MARGO (Multiproxy Approach for the Reconstruction of the Glacial Ocean surface group has focused on reconstructions for the LGM[35]. As is the case for other reconstructions, MARGO initially produced data sets for different types of records and for different regions (see ref [35] and other papers in this special issue) and subsequently provided gridded data sets at 5° by 5° resolution by averaging individual site-based reconstructions that fall into the same cell, weighted by an index of reliability [36]. Thus the MARGO gridded product contains both reconstructions and uncertainty estimates for these reconstructions. The GHOST project has produced site-based reconstructions of mean annual SST based on alkenone and magnesium/calcium palaeothermometry techniques for the MH [37].

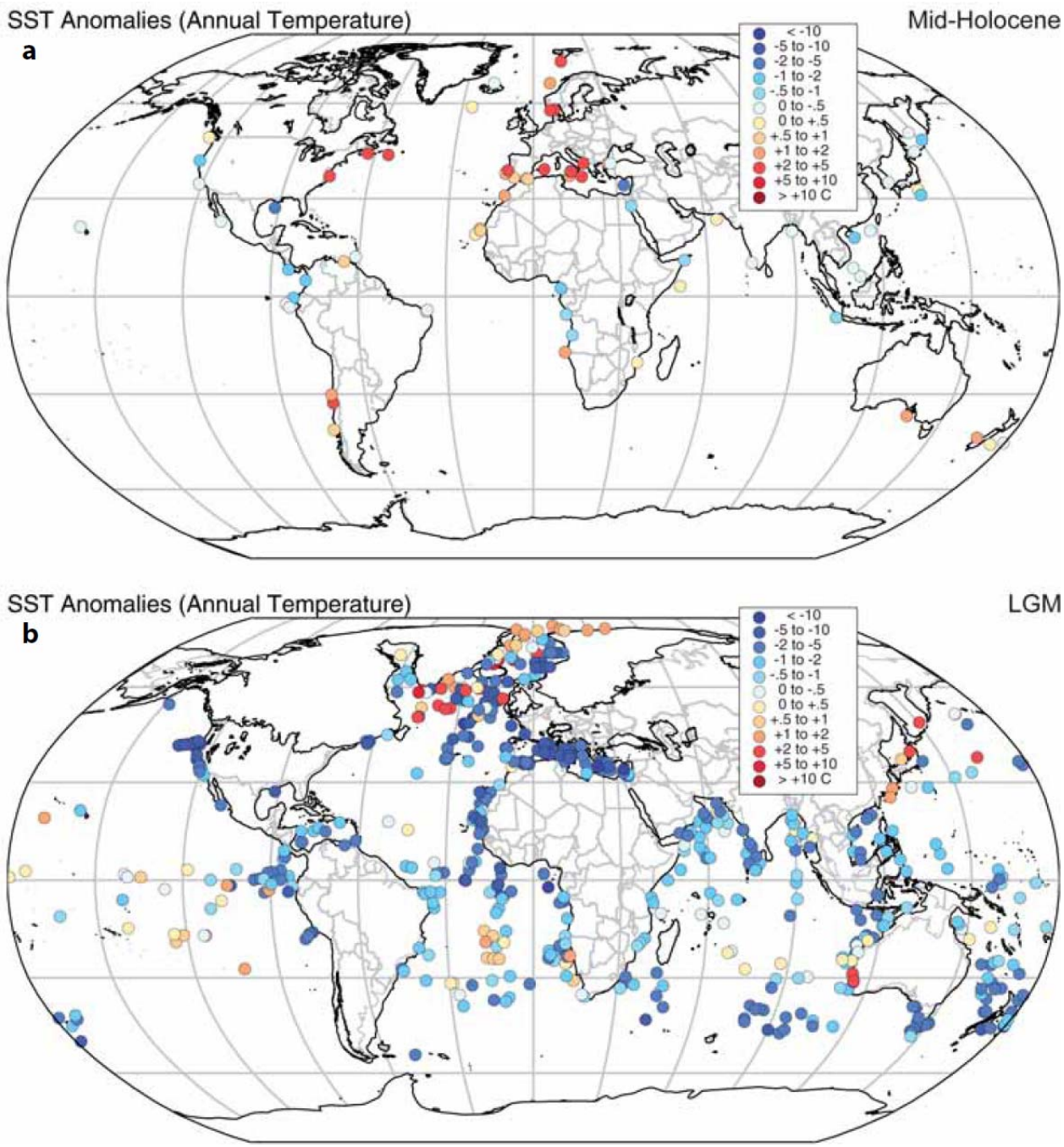

Figure S6: Changes in mean annual sea surface temperature (°C) at the (a) MH and (b) LGM from the GHOST[37] and the MARGO[36] projects respectively.

Ice cores

Land and ocean datasets are complemented by temperature estimates from Antarctic ice cores. LGM (from 20.5 to 21.5 ka) temperature changes (with respect to the mean values of the last millennium) have been estimated from Vostok, EDC, EDML, TALDICE and Dome F ice cores, in East Antarctica [38,39,40,41,42]. Ice cores were synchronized on a common age scale [43]. Temperature estimates are based on the use of the present-day isotope-temperature gradient (0.8 ‰ per °C for $\delta^{18}O$), the validity of this approach being supported by isotopic GCM simulations (see supplementary material in ref[40]). Uncertainties linked with changes in slope by ±0.1 ‰ result in uncertainties in LGM temperature change by approx. 2°C. Ice core isotopic data from each site were corrected for changes in sea water isotopic composition using estimates based on data compilation [44]. Estimates of changes in elevation (with a lower LGM central Antarctic ice sheet by approx. 100-125 m) were used to estimate the magnitude of the correction required to produce a fixed-elevation temperature estimate (enhancing the change between LGM and the present by 1 to 1.25°C). Corrections for colder LGM moisture sources (indicated by deuterium excess data) are not available for all ice cores. For EDC and EDML ice cores, this correction reduces the magnitude of LGM temperature cooling by approximately 1°C. Altogether, taking into account inter-core variability (1.4°C) and the uncertainties linked with slope (2°C), elevation (1°C) and moisture source effects (1°C), the most likely range of LGM Antarctic fixed-elevation temperature change is –10 to –6°C.

Estimates of shortwave forcing and feedbacks at the LGM

Figure 3 (main text) provides estimates of the forcing and feedbacks for different PMIP simulations (Table S2). The shortwave forcing and feedbacks were estimated using the Taylor et al. [45] approximate partial-radiative perturbation method that can be easily applied to standard model output. The method is based on a simplified shortwave radiative model of the atmosphere. Surface absorption, atmospheric scattering and absorption are represented by means of three parameters that are diagnosed at each grid cell from surface and top-of-the-atmosphere fluxes and albedo. These parameters are different in each model and simulation, and reflect the properties of the radiative code in the individual models, and the variations of these terms over different time periods. To quantify the effect of the change of each of these parameters, the parameters in the simple model are perturbed individually by the amount that they change in the climate response in order to compute the corresponding radiative change. Here, a two-sided approach is adopted, in which two estimates of the radiative change are made, considering in turn the control simulation and the paleo simulation as a reference. The average value is plotted in Figure 3.

The method is only valid for shortwave estimates and provides results in good agreement with more sophisticated approaches at the global scale (less than 7% difference) [45]. It is not possible to find a similar decomposition for longwave radiation; consequently we use a bulk estimate of the greenhouse effect computed as the difference between the surface longwave emission (which is a function of surface temperature), and the outgoing longwave radiation at the top of the atmosphere (which is attenuated relative to surface emission by greenhouse gases, water vapour and clouds). Ice-sheet and sea-level forcing values incorporate the albedo changes in regions affected by the presence of the ice-sheets at the LGM or by changes in the land-sea mask resulting from the lower sea level then. The estimate of the forcing induced by trace gases from Yoshimori et al. [46] is adopted, because the Taylor et al (2007) method does not allow a direct estimate to be made from model outputs. Therefore we consider that all the models have the same trace-gas forcing. However, the estimate of the trace-gas forcing varies by 0.4-0.6 Wm^{-2} among models in doubled-CO_2 experiments [47] which is a good approximation for the CO_2 forcing uncertainty that can be expected for the LGM simulations. The total forcing is considered as the sum of the shortwave ice sheet plus sea level forcing and trace-gas forcing, and can be compared to other estimates using an earlier version of the PMIP2 database [48] or results from one particular model [46]. The changes in topography due to

the presence of the ice-sheet, lower the surface temperature, which imposes a reduction of surface emission that can also be considered as a forcing.

The different feedbacks considered in the table concern the changes in albedo resulting from climate change, the changes in cloud cover and atmospheric absorption, and the changes in water vapor, lapse rate and clouds that affect longwave emission. For the latter we estimated the longwave feedback from the change in greenhouse effect from which we subtracted the forcing and effect of ice-sheet elevation. Each direct estimate has an error bar of about 0.2 to 0.5 Wm^{-2}, so these last numbers are only an order-of-magnitude estimates to compare different models. Changes in cloud cover account for a large fraction of the variation among the feedbacks estimated for the different models.

Table S2. Estimate of the different LGM forcing and feedback factors (Wm^{-2}) for the 6 PMIP2 models for which the necessary variables are available in the PMIP2 database. Model references can be found in Braconnot et al. [49] and on the PMIP website (http://pmip2.lsce.ipsl.fr/).

Model name	CCSM	CNRM	HadCM3M2	HadCM3M2 v	IPSL-CM4	MIROC3.2
FORCING						
Ice-sheet and see level	-2.59	-2.66	-3.23	-3.41	-3.48	-2.88
All trace gases	-2.85	-2.85	-2.85	-2.85	-2.85	-2.85
Total forcing	-5.44	-5.51	-6.08	-6.26	-6.33	-5.73
Planck emission due to orography	-3.22	-3.44	-3.21	-3.223	-3.25	-3.48
FEEDBACKS						
Surface albedo	-1.08	0.28	-1.42	-2.41	0.11	-0.26
Atmospheric absorption and scattering	-1.809	-1.09	-0.93	-0.99	-4.41	-0.06
Long wave	-2.55	-4.70	-3.72	-2.86	-2.03	-5.40

Supplementary references

[1] Berger, A. Long-term variations of caloric solar radiation resulting from the Earth's orbital elements. *Quaternary Research* **9**, 139-167 (1978).

[2] Monnin, E. *et al.* Atmospheric CO2 concentrations over the last glacial termination. *Science* **291**, 112-114 (2001).

[3] Dallenbach, A. *et al.* Changes in the atmospheric CH4 gradient between Greenland and Antarctica during the Last Glacial and the transition to the Holocene. *Geophysical Research Letters* **27**, 1005-1008, doi:10.1029/1999gl010873 (2000).
[4] Chappellaz, J. *et al.* Changes in the atmospheric CH4 gradient between Greenland and Antarctica during the Holocene. *Journal of Geophysical Research-Atmospheres* **102**, 15987-15997, doi:10.1029/97jd01017 (1997).
[5] Fluckiger, J. *et al.* Variations in atmospheric N2O concentration during abrupt climatic changes. *Science* **285**, 227-230, doi:10.1126/science.285.5425.227 (1999).
[6] Peltier, W. R. Ice age paleotopography. *Science* **265**, 195-201 (1994).
[7] Peltier, W. R. Global Glacial isostasy and the surface ot the ice-age Earth: the ICE-5G(VM2) model and GRACE. *Annual Review of Earth and Planetary Sciences* **32**, 111-149 (2004).
[8] Kohfeld, K. E. & Harrison, S. P. How well can we simulate past climates? Evaluating the models using global palaeoenvironmental datasets. *Quaternary Science Reviews* **19**, 321-346 (2000).
[9] Cheddadi, R., Yu, G., Guiot, J., Harrison, S. P. & Prentice, C. I. The climate of Europe 6000 years ago. *Climate Dynamics* **13**, 1-9 (1997).
[10] Qin, B. Q., Harrison, S. P. & Kutzbach, J. E. Evaluation of modelled regional water balance using lake status data: A comparison of 6 ka simulations with the NCAR CCM. *Quaternary Science Reviews* **17**, 535-548 (1998).
[11] Harrison, S. P., Yu, G. & Vassiljev, J. Climate changes during the holocene recorded by lakes from Europe. *Climate Development and History of the North Atlantic Realm*, 191-204 (2002).
[12] Street-Perrott, F. A. & Harrison, S. P. in *Paleoclimate Analysis and Modeling* (ed.D. Hecht) 291-340 (John Wiley, New York, 1985).
[13] Prentice, I. C., Harrison, S. P., Jolly, D. & Guiot, J. The climate and biomes of Europe at 6000 yr BP: Comparison of model simulations and pollen-based reconstructions. *Quaternary Science Reviews* **17**, 659-668 (1998).
[14] Prentice, I. C., Guiot, J., Huntley, B., Jolly, D. & Cheddadi, R. Reconstructing biomes from palaeoecological data: a general method and its application to European pollen data at 0 and 6 ka. *Climate Dynamics* **12**, 185-194 (1996).
[15] Prentice, I. C. & Jolly, D. Mid-Holocene and glacial-maximum vegetation geography of the northern continents and Africa. *Journal of Biogeography* **27**, 507-519 (2000).
[16] Harrison, S. P., Yu, G., Takahara, H. & Prentice, I. C. Palaeovegetation - Diversity of temperate plants in east Asia. *Nature* **413**, 129-130 (2001).
[17] Bigelow, N. H. *et al.* Climate change and Arctic ecosystems: 1. Vegetation changes north of 55 degrees N between the last glacial maximum, mid-Holocene, and present. *Journal of Geophysical Research-Atmospheres* **108** (2003).
[18] Pickett, E. J. *et al.* Pollen-based reconstructions of biome distributions for Australia, Southeast Asia and the Pacific (SEAPAC region) at 0, 6000 and 18,000 (14)C yr BP. *Journal of Biogeography* **31**, 1381-1444, doi:10.1111/j.1365-2699.2004.01001.x (2004).
[19] Marchant, R. *et al.* Pollen-based biome reconstructions for Latin America at 0, 6000 and 18 000 radiocarbon years ago. *Climate of the Past* **5**, 725-767 (2009).
[20] Liu, Z. Y., Wang, Y., Gallimore, R., Notaro, M. & Prentice, I. C. On the cause of abrupt vegetation collapse in North Africa during the Holocene: Climate variability vs. vegetation feedback. *Geophysical Research Letters* **33**, doi:L22709 10.1029/2006gl028062 (2006).
[21] Harrison, S. P. *et al.* Intercomparison of Simulated Global Vegetation Distributions in Response to 6 kyr BP Orbital Forcing. *Journal of Climate* **11**, 2721-2742 (1998).

[22] Wohlfahrt, J. *et al.* Evaluation of coupled ocean-atmosphere simulations of the mid-Holocene using palaeovegetation data from the northern hemisphere extratropics. *Climate Dynamics* **31**, 871-890, doi:DOI 10.1007/s00382-008-0415-5 (2008).
[23] Prentice, I. C., Harrison, S. P. & Bartlein, P. J. Global vegetation and terrestrial carbon cycle changes after the last ice age. *New Phytologist* **189**, 988-998, doi:10.1111/j.1469-8137.2010.03620.x (2011).
[24] Power, M. J. *et al.* Changes in fire regimes since the Last Glacial Maximum: an assessment based on a global synthesis and analysis of charcoal data. *Climate Dynamics* **30**, 887-907, doi:10.1007/s00382-007-0334-x (2008).
[25] Power, M. J., Marlon, J. R., Bartlein, P. J. & Harrison, S. P. Fire history and the Global Charcoal Database: A new tool for hypothesis testing and data exploration. *Palaeogeography Palaeoclimatology Palaeoecology* **291**, 52-59, doi:10.1016/j.palaeo.2009.09.014 (2010).
[26] Marlon, J. R. *et al.* Climate and human influences on global biomass burning over the past two millennia. *Nature Geoscience* **1**, 697-702, doi:10.1038/ngeo313 (2008).
[27] Kleinen, T., Tarasov, P., Brovkin, V., Andreev, A. & Stebich, M. Comparison of modeled and reconstructed changes in forest cover through the past 8000 years: Eurasian perspective. *Holocene* **21**, 723-734, doi:10.1177/0959683610386980 (2011).
[28] Prentice, I. C. *et al.* Modeling fire and the terrestrial carbon balance. *Global Biogeochemical Cycles* **25**, doi:Gb3005 10.1029/2010gb003906 (2011).
[29] Mahowald, N. *et al.* Dust sources and deposition during the last glacial maximum and current climate: A comparison of model results with paleodata from ice cores and marine sediments. *Journal of Geophysical Research-Atmospheres* **104**, 15895-15916 (1999).
[30] Jansen, E. *et al.* in *Climate Chane 2007: The Physical Science Basis. Contribution of Working Group I to the Fourth Assessement Report of the Intergovernmental Panel on Climate Change* eds S. Solomon *et al.*) (Cambridge University Press, 2007).
[31] Werner, M. *et al.* Seasonal and interannual variability of the mineral dust cycle under present and glacial climate conditions. *Journal of Geophysical Research-Atmospheres* **107** (2002).
[32] Kohfeld, K. E. & Harrison, S. P. DIRTMAP: the geological record of dust. *Earth-Science Reviews* **54**, 81-114 (2001).
[33] Maher, B. A. & Kohfeld, K. 'DIRTMAP' Version 3, LGM and late Holocene Aeolian Fluxes from Ice Cores, Marine Sediment Traps, Marine Sediments and Loess Deposits. *http://www.lec.lancs.ac.uk/dirtmap3* (2009).
[34] Bartlein, P. J. *et al.* Pollen-based continental climate reconstructions at 6 and 21 ka: a global synthesis. *Climate Dynamics* **37**, 775-802, doi:10.1007/s00382-010-0904-1 (2011).
[35] Kucera, M., Rosell-Mele, A., Schneider, R., Waelbroeck, C. & Weinelt, M. Multiproxy approach for the reconstruction of the glacial ocean surface (MARGO). *Quaternary Science Reviews* **24**, 813-819, doi:DOI 10.1016/j.quascirev.2004.07.017 (2005).
[36] Waelbroeck, C. *et al.* Constraints on the magnitude and patterns of ocean cooling at the Last Glacial Maximum. *Nature Geoscience* **2**, 127-132, doi:Doi 10.1038/Ngeo411 (2009).
[37] Leduc, G., Schneider, R., Kim, J. H. & Lohmann, G. Holocene and Eemian sea surface temperature trends as revealed by alkenone and Mg/Ca paleothermometry. *Quaternary Science Reviews* **29**, 989-1004, doi:DOI 10.1016/j.quascirev.2010.01.004 (2010).
[38] Masson-Delmotte, V. *et al.* A comparison of the present and last interglacial periods in six Antarctic ice cores. *Climate of the Past* **7**, 397-423, doi:10.5194/cp-7-397-2011 (2011).
[39] Kawamura, K. *et al.* Northern Hemisphere forcing of climatic cycles in Antarctica over the past 360,000 years. *Nature* **448**, 912-915 (2007).
[40] Jouzel, J. *et al.* Orbital and millennial Antarctic climate variability over the past 800,000 years. *Science* **317**, 793-796, doi:DOI 10.1126/science.1141038 (2007).

[41] Vimeux, F., Cuffey, K. M. & Jouzel, J. New insights into Southern Hemisphere temperature changes from Vostok ice cores using deuterium excess correction. *Earth and Planetary Science Letters* **203**, 829-843 (2002).
[42] Stenni, B. *et al.* Expression of the bipolar see-saw in Antarctic climate records during the last deglaciation. *Nature Geoscience* **4**, 46-49, doi:10.1038/ngeo1026 (2011).
[43] Lemieux-Dudon, B. *et al.* Consistent dating for Antarctica and Greenland ice cores. *Quaternary Science Reviews* **29**, 8-20 (2010).
[44] Bintanja, R., van de Wal, R. & Oerlemans, J. Modelled atmospheric temperatures and global sea levels over the past million years. *Nature* **437**, 125-128 (2005).
[45] Taylor, K. E. *et al.* Estimating shortwave radiative forcing and response in climate models. *Journal of Climate* **20**, 2530-2543 (2007).
[46] Yoshimori, M., Yokohata, T. & Abe-Ouchi, A. A Comparison of Climate Feedback Strength between CO2 Doubling and LGM Experiments. *Journal of Climate* **22**, 3374-3395, doi:Doi 10.1175/2009jcli2801.1 (2009).
[47] Meehl, G. A. *et al.* in *Climate Change 2007 : The Physical Science Basis. Contribution of Working Group I to the Fourth Assessment Report of the Intergovernmental Panel on Climate Change* (ed S. Solomon, D. Qin, M. Manning, Z. Chen, M. Marquis, K.B. Averyt, M. Tignor and H.L. Miller) (Cambridge University Press, 2007).
[48] Crucifix, M. Does the Last Glacial Maximum constrain climate sensitivity? *Geophysical Research Letters* **33**, - (2006).
[49] Braconnot, P. *et al.* Results of PMIP2 coupled simulations of the Mid-Holocene and Last Glacial Maximum - Part 1: experiments and large-scale features. *Climate of the Past* **3**, 261-277 (2007).